Electronic Supplementary Information

Modified potential for atomistic simulation of the growth of carbon materials from binary alloy catalysts

Jaewoong Hur [a*]

[a] Center for Multidimensional Carbon Materials (CMCM), Institute for Basic Science (IBS), Ulsan, 44919 Republic of Korea

*Corresponding author

E-mail address: jwhur75@unist.ac.kr, jwhur75@gmail.com

■ Understanding of the newly modified potential using binary alloy catalyst

The potential energies of all types of carbon materials using binary alloy catalyst can be obtained from three terms like below;

$$E^{TOT} = E^{CM} + E^{CC} + E^{MM} \tag{S1}$$

where E^{CM}, E^{CC}, and E^{MM} are carbon-metal (C-M), carbon-carbon (C-C), and metal-metal (M-M) interaction energy terms, respectively. E^{TOT} is estimated by using the three potential energy terms, and these three terms can be described as below;

$$E^{CM} = \sum_{i} \sum_{j>i} E_{ij}^{CM_{1st}} + \sum_{i} \sum_{j>i} E_{ij}^{CM_{2nd}} \tag{S2}$$

$$E^{CC} = \sum_{i} \sum_{j>i} E_{ij}^{CC} \tag{S3}$$

$$E^{MM} = \sum_{i} \sum_{j>i} E_{ij}^{M_{1st}M_{1st}} + \sum_{i} \sum_{j>i} E_{ij}^{M_{1st}M_{2nd}} + \sum_{i} \sum_{j>i} E_{ij}^{M_{2nd}M_{2nd}} \tag{S4}$$

For C-M interactions around C-C bonding materials, each of the binary alloy metals (i.e. named M_{1st} as Pt or M_{2nd} as Cu in the Pt-Cu binary metal alloy) leads to C-M_{1st} or C-M_{2nd} interactions, which were newly implemented in the new hybrid reactive empirical potential, taking place at any bonding environment of carbons, and hence those chemical interactions were considered in this work. REBO potential was employed for C-C interaction energy estimations[1], and the cases were also considered to be involved in the presence of bimetallic alloy catalyst. For M-M potential functions, bimetallic alloy interactions were newly implemented by benchmarking a long-range Finnis-Sinclair potential algorithm for using binary alloy metals.[2]

- **C-M_{1st} / C-M_{2nd} interactions based on binary alloy catalyst**

$E_{ij}^{CM}(r_{ij})$ term contains both C-M_{1st} and C-M_{2nd} interaction energy terms, which are composed of the distance dependence term $E_D^{CM}(r_{ij})$ and the angle dependence term $E_\theta^{CM}(r_{ik}, r_{il}, \theta_{lik})$ that estimates the angle contribution of C-M_{1st} / C-M_{2nd} bonding configurations.

$$E_{ij}^{CM}(r_{ij}) = E_D^{CM}(r_{ij}) + E_\theta^{CM}(r_{ik}, r_{il}, \theta_{lik}) \quad \text{(S5)}$$

a) Distance dependence term

Morse type repulsive and attractive potentials were used to describe the distance dependence of C-M_{1st} / C-M_{2nd} interactions.[3]

$$E_D^{CM}(r_{ij}) = \alpha_D^{CM}\left[V^R(r_{ij}) - V^A(r_{ij})\right] \quad \text{(S6)}$$

$$V^R(r_{ij}) = f^{CM}(r_{ij})\frac{D_e}{S-1}exp^{-\beta\sqrt{2S}(r_{ij}-R_e)} \quad \text{(S7)}$$

$$V^A(r_{ij}) = f^{CM}(r_{ij})\frac{D_e S}{S-1}exp^{-\beta\sqrt{\frac{2}{S}}(r_{ij}-R_e)} \quad \text{(S8)}$$

where $f^{CM}(r_{ij}) = \delta_{xC}f^{CM_{1st}}(r_{ij}) + \delta_{(1-x)C}f^{CM_{2nd}}(r_{ij})$: δ_{ij} represents a metal distinct notation

$$\begin{cases}\delta_{xC} = 1 \\ \delta_{(1-x)C} = 0\end{cases}, \ if\ x = 1 \text{ and } \quad \begin{cases}\delta_{xC} = 0 \\ \delta_{(1-x)C} = 1\end{cases}, \ if\ x = 0 \quad \text{(S9)}$$

D_e and R_e are the equilibrium binding energy and bond distance between *i* and *j*, and the values are calculated with functions of an average atomic coordination number N_{ij} including parameters. The parameters D_{e1}, D_{e2}, R_{e1}, R_{e2} used for C-M_{1st} / C-M_{2nd} bond formations and the other parameters S, β, C_D, C_R all components of the Morse type potentials are displayed in Table S1. In addition, λ is the parameter for distinct contributions of the local carbon environment around C-M bonding configurations.

$$D_e = D_{e1} + D_{e2}\, exp\left[-C_D(N_{ij})\right] \tag{S10}$$

$$R_e = R_{e1} - R_{e2}\, exp\left[-C_R(N_{ij})\right] \tag{S11}$$

$$N_{ij} = N_i^{M_{1st}+M_{2nd}} + \lambda N_j^C \tag{S12}$$

$$N_i^{M_{1st}+M_{2nd}} = \sum_{k\neq j}^{metal} f^{CM_{1st}}(r_{ik}) + \sum_{k\neq j}^{metal} f^{CM_{2nd}}(r_{ik}) \tag{S13}$$

$$N_j^C = \sum_{l\neq i} f^{CC}(r_{jl}) \tag{S14}$$

$N_i^{M_{1st}+M_{2nd}}$ represents the neighbors of atom *i* as counting each of binary alloy metals. The composition of bimetallic alloy catalyst might also be expressed as $N_i^{M_{1st}+M_{2nd}} = N_i^{M_x+M_{(1-x)}}$.

Table S1. Parameters for C-M_{1st} and C-M_{2nd} interactions using Morse type potentials with Pt-Cu alloy catalyst.

Parameters for C-M_{1st} bonds	Parameters for C-M_{2nd} bonds
$D_{e1}(eV) = 2.65$	$D_{e1}(eV) = 2.50$
$D_{e2}(eV) = 2.25$	$D_{e2}(eV) = 1.90$
$C_D = 0.90$	$C_D = 0.60$
$R_{e1}(\text{Å}) = 1.85$	$R_{e1}(\text{Å}) = 1.95$
$R_{e2}(\text{Å}) = 0.15$	$R_{e2}(\text{Å}) = 1.80$
$C_R = 0.50$	$C_R = 0.50$
$S = 1.40$	$S = 1.40$
Weighting parameter for the local environment around C-M bonds	
$\lambda = 0.08$	

The number of neighboring alloy metals can be counted by summing switching functions. And, the cut-off functions of the C-M_{1st} and C-M_{2nd} interactions are expressed like below in terms of atom *i* side;

$$f^{CM_{1st}}(r_{ik}) = \begin{cases} 1 & , \quad r_{ik} < R_{CM_{1st,min}} \\ \dfrac{\left(1 + cos\left(\pi \cdot \dfrac{r_{ik} - R_{CM_{1st,min}}}{R_{CM_{1st,max}} - R_{CM_{1st,min}}}\right)\right)}{2} & , \quad R_{CM_{1st,min}} < r_{ik} < R_{CM_{1st,max}} \\ 0 & , \quad r_{ik} > R_{CM_{1st,max}} \end{cases} \tag{S15}$$

$$f^{CM_{2nd}}(r_{ik}) = \begin{cases} 1 & , \quad r_{ik} < R_{CM_{2nd,min}} \\ \dfrac{\left(1 + cos\left(\pi \cdot \dfrac{r_{ik} - R_{CM_{2nd.min}}}{R_{CM_{2nd,max}} - R_{CM_{2nd,min}}}\right)\right)}{2}, & R_{CM_{2nd,min}} < r_{ik} < R_{CM_{2nd,max}} \\ 0 & , \quad r_{ik} > R_{CM_{2nd,max}} \end{cases} \tag{S16}$$

In terms of counting C-C covalent bonding descriptions as the neighbors of atom *j*, N_j^C, the function $f^{CC}(r_{jl})$ limits the range of the covalent bonding interactions, and the parameter fitting for carbons assumes a value of one for $f^{CC}(r_{jl})$ for nearest neighbors and zero for all other interatomic distances.

$$f^{CC}(r_{jl}) = \begin{cases} 1 & , \quad r_{jl} < R_{CC_{min}} \\ \dfrac{\left(1 + cos\left(\pi \cdot \dfrac{r_{jl} - R_{CC_{min}}}{R_{CC_{max}} - R_{CC_{min}}}\right)\right)}{2}, & R_{CC_{min}} < r_{jl} < R_{CC_{max}} \\ 0 & , \quad r_{jl} > R_{CC_{max}} \end{cases} \tag{S17}$$

where $R_{CC_{min}}$ and $R_{CC_{max}}$ are cut-off distances.

Table S2. Parameters for $f^{CM_{1st\,/\,2nd}}(r_{ik})$ and $f^{CC}(r_{jl})$ based on Pt-Cu alloy catalyst.

$R_{CM_{1st,min}}(\text{Å}) = 2.2$	$R_{CM_{1st,max}}(\text{Å}) = 2.7$
$R_{CM_{2nd,min}}(\text{Å}) = 2.3$	$R_{CM_{2nd,max}}(\text{Å}) = 2.8$
$R_{CC_{min}}(\text{Å}) = 1.7$	$R_{CC_{max}}(\text{Å}) = 2.0$

α_D^{CM} term treats the effects of the local bonding environment around the C-M_{1st} and C-M_{2nd} bonds. $N_i^{C_1}$ is the number of nearest carbon neighboring atoms, and $N_i^{C_2}$ is the number of next nearest carbon neighboring atoms around atom *i*. And, N_i^M is the number of metal neighboring atoms around carbon atom *i*. Different compositions of $\left(N_i^{C_1}, N_i^{C_2}, N_i^M\right)$ indicate different local bonding environment cases.

$$\alpha_D^{CM} = \alpha_D^{CM}\left(N_i^{C_1}, N_i^{C_2}, N_j^M\right) \tag{S18}$$

$$N_i^{C_1} = \sum_{k \neq j,m}^{carbon} f^{CC}{}_{ik}(r_{ik}) \tag{S19}$$

$$N_i^{C_2} = \sum_{l \neq j,m,k}^{carbon} f^{CC}{}_{il}(r_{il}) \tag{S20}$$

$$N_i^M = N_i^{M_{1st}+M_{2nd}} = \sum_{m \neq j}^{metal} f^{CM_{1st}}(r_{im}) + \sum_{m \neq j}^{metal} f^{CM_{2nd}}(r_{im}) \tag{S21}$$

$N_i^{C_1}$, $N_i^{C_2}$, N_i^M also need parameterization, and with tricubic spline functions, the spline knots of α_D^{CM} can be interpolated. Therefore, the effects of the local bonding environment around C-M_{1st} / C-M_{2nd} bonding configurations can be considered from α_D^{CM} parameterization.

b) Angle dependence term

The angle dependence term was benchmarked to the newly modified hybrid potential from the previous C-M potential[4] to implement further angular bonding configurations for C-M_{1st} and C-M_{2nd} bond angles such as the edges of a graphene nanoribbon on the bimetallic alloy metal catalyst surface.

$$E_\theta^{CM}(r_{ik}, r_{il}, \theta_{lik}) = \sum_i \left[\alpha_{lik}\left(N_i^{C_1}, N_i^{C_2}\right)\left(\vec{V}_{C_i} \cdot \vec{V}_{M_i}\right)\right] \tag{S22}$$

$$\vec{V}_{C_i} = \sum_{l \neq j}^{carbon} f^{CC}(r_{il})(\vec{r}_l - \vec{r}_i) \tag{S23}$$

$$\vec{V}_{M_i} = \sum_{k \neq l,j}^{metal} f^{CM_{1st}}(r_{ik}) + \sum_{k \neq l,j}^{metal} f^{CM_{2nd}}(r_{ik})\,(\vec{r}_k - \vec{r}_i) \tag{S24}$$

$$\vec{V}_{C_i} \cdot \vec{V}_{M_i} = \sum_{l \neq k,j} f^{CC}(r_{il}) \left(\sum_{k \neq l,j} f^{CM_{1st}}(r_{ik}) + \sum_{k \neq l,j} f^{CM_{2nd}}(r_{ik}) \right) \sum_{lik} r_{il} r_{ik} cos(\theta_{lik}) \tag{S25}$$

where θ_{lik} is the angle between the C_i-C_l bond and the C_i-M_k bond (C_l-C_i-C_k). Depending on $\theta_{lik}(0 \leq \theta \leq \pi)$, the inner product of $\vec{V}_{C_i} \cdot \vec{V}_{M_i}$ is determined. Similar to the concept of α_D^{CM}, α_{lik} is a function of $\left(N_i^{C_1}, N_i^{C_2}\right)$ that counts the number of carbon neighboring atoms around C_i and determines the magnitude of the angle necessary for any of different types of carbon materials.

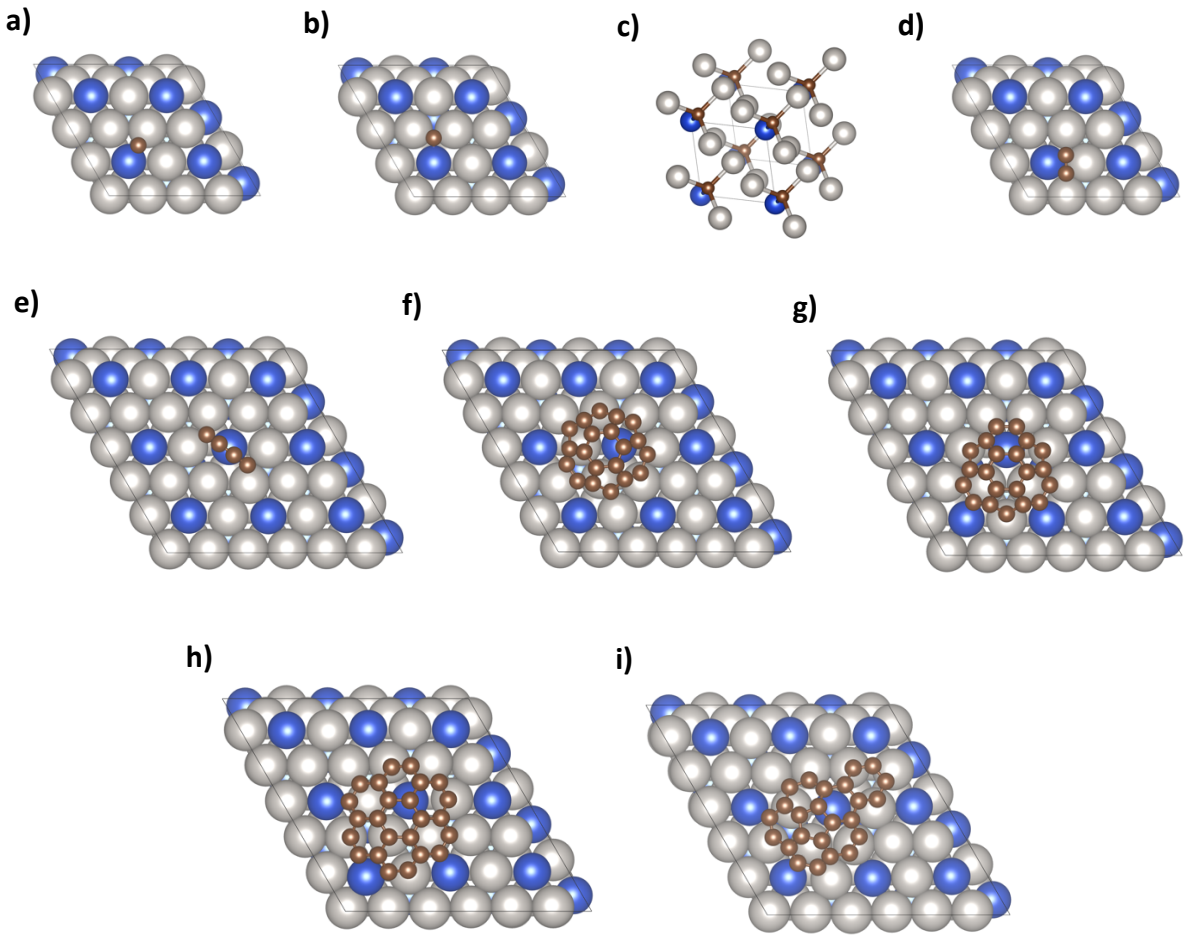

Fig. S1 Bonding configurations for different C-M_{1st} and C-M_{2nd} interactions between carbons and $Pt_3Cu(111)$ bimetallic catalyst: **a)** and **b)** C_1, **c)** C_1 in Pt-Cu bulk alloy catalyst, **d)** dimer, **e)** chain, **f)** C_{20}, **g)** C_{21}, **h)** $C_{24}(D_{6h})$ **i)** $C_{24}(C_s)$. Carbons displayed in **a)**, **b)**, **d)**, **e)**, **f)**, **g)**, **h)**, **i)** are all on the surface of $Pt_3Cu(111)$ binary catalyst.

Table S3. C-M_{1st} and C-M_{2nd} bond formation energies (E_f) for different types of carbon materials based on Pt-Cu alloy catalyst.

Species	$N_j^{C_{1st}}$	$N_j^{C_{2nd}}$	$N_j^{M_{1st}/M_{2nd}}$		$E_f(eV)^*$		Error (%)
			$N_j^{M_{1st}}$	$N_j^{M_{2nd}}$	new FF	PBE	
C_1	0	0	1	1	-5.42	-5.21	4.09

C_1	0	0	2	1	-6.13	-6.42	4.62
C_1	0	0	3	1	-7.11	-6.83	4.07
C_2	1	0	2	1	-5.45	-5.27	3.48
Chain	1,2	1	1,2	1	-6.32	-6.17	2.42
C_{20}	2,3	3,4,6	1,2,3	0,1	-16.67	-16.19	2.99
C_{21}	2,3	3,4,6	1,2,3	0,1	-17.72	-18.68	5.17
C_{24} (D_{6h})	2,3	3,4,6	1,2,3	0,1	-16.13	-15.37	4.94
C_{24} (C_s)	2,3	2,3,4,5,6	1,2,3	0,1	-14.79	-14.27	3.61

$* E_{f(C-M)} = E(N*C + N*M_{1st} + N*M_{2nd}) - E(N*C) - E(N*M_{1st} + N*M_{2nd})$ where N is the number of atoms for each of carbon and bimetal elements such as Pt or Cu in this work. Since the ratio of Pt and Cu is 3 to 1 for the PES calculations in considering $N_i^{M_{1st}}$and $N_i^{M_{2nd}}$, $N_i^{M_{1st}}$ has three maximum neighboring atoms, but $N_i^{M_{2nd}}$ has either one neighboring atom or none counting on the first layer surface of bimetallic alloy catalyst.

Different bonding configurations to calculate various C-M_{1st} and C-M_{2nd} interaction energies between representative carbon materials and Pt-Cu alloy catalyst, displayed in Fig. S1, were used for the accurate PES descriptions of the newly developed potential. Structural bonding environment between C_1 and binary alloy catalyst (i.e. Pt-Cu) was considered as the PES fitting set to define the bonding characteristics which are also necessary for the CNTs growth in MD simulations. Overall, Table S3 illustrates the bond formation energies of the fitting set, as compared to DFT energy, using different bonding configurations between C_1 and binary metal catalyst. Also, the energetics of the validation set are included in Table S3, which represents dimer, chain, C_{20}, C_{21}, $C_{24}(D_{6h})$, and $C_{24}(C_s)$ with a different point group symmetry using new parameterization and reparameterization for C-M_{1st} and C-M_{2nd} interactions.

- **C-C interactions with the neighbors of binary alloy metals**

REBO potential was used for the description of C-C bonding interactions where $V^R(r_{ij})$ and $V^A(r_{ij})$ terms represent repulsive and attractive potentials. The two $V^R(r_{ij})$ and $V^A(r_{ij})$ potential terms mainly depend on the distance r_{ij} between atoms *i* and *j*, and also E_{ij}^{REBO} values rely on the coordination number close to the $i-j$ bond. In addition, α_{ij}^{CC} is provided as a

function to reflect the C-M_{1st} / C-M_{2nd} bonding interactions using alloy metals around the C-C bonds.

$$E_{ij}^{CC} = \alpha_{ij}^{CC}\left[V^R(r_{ij}) - V^A(r_{ij})\right] \tag{S26}$$

$$V^R(r_{ij}) = f^{CC}(r_{ij})\left[\left(1+\frac{Q}{r_{ij}}\right)Ae^{-\alpha r_{ij}}\right] \tag{S27}$$

$$V^A(r_{ij}) = b_{ij}f^{CC}(r_{ij})\sum_{n=1,3} B_n e^{-\beta_n r_{ij}} \tag{S28}$$

where Q, A, α, β_n, and B_n are parameters used in REBO potential to describe repulsive and attractive interactions of atom pairs. b_{ij} is an important term to describe intramolecular interactions of carbon materials, depending on bond distance, bond angle, dihedral angle for sp^2 hybridized carbon configurations, and local bonding environments of atoms *i* and *j*.

$$b_{ij} = \frac{1}{2}\left[b_{ij}^{\sigma\pi} + b_{ji}^{\sigma\pi}\right] + \prod_{ij}^{RC} + b_{ij}^{DH} \tag{S29}$$

$$b_{ij}^{\sigma\pi} = \left[1 + \sum_{k\neq i,j} f_{ik}^{CC}(r_{ik})G\left(cos(\theta_{ijk})\right)e^{\lambda_{ijk}} + P_{ij}(N_{ij}^C, N_{ij}^H)\right]^{-1/2} \tag{S30}$$

In equation S30, the function *P* represents a bicubic spline, and the quantities of N_{ij}^C and N_{ij}^H represent the number of carbon and hydrogen atoms, respectively that are neighbors of atom *i* and *j*. However, N_{ij}^C term is only considered for the function *P* in this study, because different types of carbon materials have only been utilized. And, the rest of the b_{ij} term and all parameters used in REBO potential are more detailed in the reference.[1] As the similar concept of α_D^{CM} term, α_{ij}^{CC} term reflects the presence of the Pt-Cu alloy catalyst around C-C bond circumstance, and is expressed like below.

$$\alpha_{ij}^{CC} = \begin{cases} 1 & , \quad N_{ij}^{M} < N_{min}^{M} \\ \dfrac{\left(1 + cos\left(\pi \cdot \dfrac{N_{ij}^{M} - N_{min}^{M}}{N_{max}^{M} - N_{min}^{M}}\right)\right)}{2} & , \quad N_{min}^{M} < N_{ij}^{M} < N_{max}^{M} \\ 0 & , \quad N_{ij}^{M} > N_{max}^{M} \end{cases} \tag{S31}$$

$$N_{ij}^{M} = \left(N_{i}^{M_{1st}+M_{2nd}} + N_{j}^{M_{1st}+M_{2nd}}\right)/2 \tag{S32}$$

where N_{ij}^{M} is the averaged alloy metal neighbors of atoms *i* and *j* as counting binary metal environments around C-C bonds. Also, $N_{min}^{M} = 2.0$ and $N_{max}^{M} = 6.0$ represent the cut-off numbers of the metal neighboring atoms.

- **M-M interactions**

The total internal energy of an elemental material is calculated by the long-range Finnis-Sinclair potentials equation which was proposed by Sutton and Chen[5] :

$$E^{FS} = \varepsilon \left[\frac{1}{2}\sum_{i}\sum_{j(j>i)} V(r_{ij}) - c\sum_{i}\rho_{i}^{1/2}\right] \tag{S33}$$

In equation S33, $V(r_{ij})$ describes a two-body repulsive interaction between atoms *i* and *j*, separated by a distance r_{ij}, and many-body term is purely cohesive. In implementing the square root term in the FS potential, the motivation comes from an analogy of the second moment approximation to the tight-binding model representing the cohesive many-body contribution by the square root of its coordination number.[6] The functions ρ_i give van der Waals pair contribution to take the long-range interactions into account between atoms at large separations and *N*-body covalent bonding interactions at small separations by using an inverse sixth power. Both repulsive and attractive contributions to the total energy depend only upon the interatomic separations. While the potential descriptions of elemental metal interactions are mentioned

above, it is also known that the descriptions of binary A-B alloys as for solid metal surface relaxations have been reported[2], and further with small changes the descriptions having the same concept as the previous model can be expressed like below,

$$E^{FS} = \left[\sum_i \sum_{j>i} \alpha\varepsilon^{AA}\left[\frac{a^{AA}}{r}\right]^{n^{AA}} + \beta\varepsilon^{BB}\left[\frac{a^{BB}}{r}\right]^{n^{BB}} + \gamma\varepsilon^{AB}\left[\frac{a^{AB}}{r}\right]^{n^{AB}}\right]$$
$$-\alpha\varepsilon^{AA}c^{AA}\sum_i\left[\sum_{j>i}\alpha\left[\frac{a^{AA}}{r}\right]^{m^{AA}} + \gamma\left[\frac{a^{AB}}{r}\right]^{m^{AB}}\right]^{\frac{1}{2}} \quad \text{(S34)}$$
$$-\beta\varepsilon^{BB}c^{BB}\sum_i\left[\sum_{j>i}\beta\left[\frac{a^{BB}}{r}\right]^{m^{BB}} + \gamma\left[\frac{a^{AB}}{r}\right]^{m^{AB}}\right]^{\frac{1}{2}}$$

where α, β, γ are parameters to distinguish the pair metal interactions one another. $\varepsilon^{AA}, c^{AA}, a^{AA}, m^{AA}$, and n^{AA} are created via the parameters $\varepsilon, c, a, m,$ and n of the pure A metal, and similarly, $\varepsilon^{BB}, c^{BB}, a^{BB}, m^{BB}$, and n^{BB} are also produced with the parameters $\varepsilon, c, a, m,$ and n of the pure B metal. Thus, only the four parameters $\varepsilon^{AB}, a^{AB}, m^{AB}$, and n^{AB} remain to be determined. Since the definitions of the functions are like below,

$$\varepsilon^{AA}\left[\frac{a^{AA}}{r}\right]^{n^{AA}} = V^{AA}(r), \qquad \varepsilon^{BB}\left[\frac{a^{BB}}{r}\right]^{n^{BB}} = V^{BB}(r), \qquad \varepsilon^{AB}\left[\frac{a^{AB}}{r}\right]^{n^{AB}} V^{AB}(r) \quad \text{(S35)}$$

$$\left[\frac{a^{AA}}{r}\right]^{m^{AA}} = \emptyset^{AA}(r), \qquad \left[\frac{a^{BB}}{r}\right]^{m^{BB}} = \emptyset^{BB}(r), \qquad \left[\frac{a^{AB}}{r}\right]^{m^{AB}} = \emptyset^{AB}(r) \quad \text{(S36)}$$

these parameters are obtained from assuming that the functions V^{AB} may be derived as followings:

$$V^{AB} = (V^{AA}V^{BB})^{1/2} \text{ and } \emptyset^{AB} = (\emptyset^{AA}\emptyset^{BB})^{1/2} \quad \text{(S37)}$$

These relations create the following expressions for the rest of parameters:

$$m^{AB} = \frac{1}{2}(m^{AA} + m^{BB}), \qquad n^{AB} = \frac{1}{2}(n^{AA} + n^{BB}), \quad \text{(S38)}$$

$$a^{AB} = (a^{AA}a^{BB})^{1/2}, \qquad \varepsilon^{AB} = (\varepsilon^{AA}\varepsilon^{BB})^{1/2} \tag{S39}$$

Table S4. Parameters for M-M interactions using Finnis-Sinclair potentials based on Pt-Cu bimetallic alloy catalyst.

Parameters for M_{1st}-M_{1st} bonds					
$\varepsilon_{11}(eV)$	c_{11}	$a_{11}(\text{Å})$	m	n	α
0.019835	34.428	3.92	8	10	1.021
Parameters for M_{2nd}-M_{2nd} bonds					
$\varepsilon_{22}(eV)$	c_{22}	$a_{22}(\text{Å})$	m	n	β
0.012386	39.755	3.61	6	9	1.021
Parameters for M_{1st}-M_{2nd} bonds					
$\varepsilon_{12}(eV)$	$a_{12}(\text{Å})$	m	n	γ	
0.015670	3.88	7	9.5	1.021	

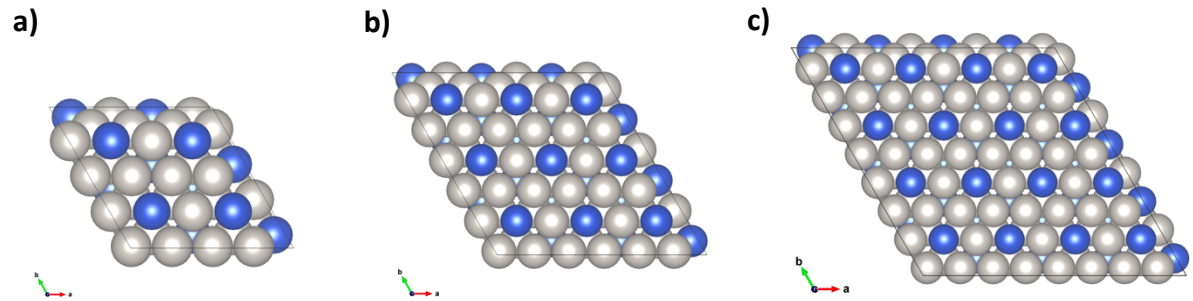

Fig. S2 Bonding configurations for different M-M interactions of $Pt_3Cu(111)$ alloy catalyst: **a)** 4x4 unit cell, **b)** 6x6 unit cell, and **c)** 8x8 unit cell. **a)**, **b)**, and **c)** all consist of $Pt_3Cu(111)$ catalyst.

With M-M parameterization given in Table S4, binary alloy interatomic interactions are described by equation S34 and functions S35 and S36. Binary M-M interactions contributed to bond formation energies summarized in Table S5 depend on the structural bonding configurations shown in Fig. S2 where the ratio of Pt and Cu is 3 to 1 having (111) Miller indices of crystal structure.

Table S5. M-M bond formation energies (E_f) between Pt and Cu alloy catalyst.

	$E_f(eV)^*$ per atom		
$Pt_3Cu(111)$	new FF	PBE	Error (%)
4x4	-4.861	-4.860	0.02
6x6	-4.883	-4.859	0.49

8x8	-4.931	-4.861	1.42

$* E_{f(M-M)} = E(N * M_{1st} + N * M_{2nd}) - E(N * M_{1st}) - E(N * M_{2nd})$ where N is the number of atoms for each of bimetal components such as Pt or Cu in this research.

In the meantime, in order to validate whether the new approach implemented in the modified hybrid potential code also works well for the interactions between carbons and single metal catalyst, each of the elemental metal catalysts (i.e. Pt or Cu) has been used with its reparameterization.

■ Validation of the newly modified approach using an elemental catalyst

- **C-M_{1st} interactions based on only Pt catalyst**

For the validations of the newly modified potential treating the C-M_{1st} interactions between selected carbons and a pure Pt catalyst, all the necessary parameters given in Table S6 and Table S7 were adjusted to calculate C-M_{1st} and the C-C interaction energies of C_1, (4,4), and (7,0), based on different bonding configurations with the pure Pt metal catalyst.

Table S6. Parameters for $f^{CM_{1st}}(r_{ik})$, $f^{CC}(r_{ij})$, and α_{ij}^{CC} term reflecting the presence of elemental Pt catalyst here named M_{1st}.

$R_{CM_{1st,min}}(\text{Å}) = 2.4$	$R_{CM_{1st,max}}(\text{Å}) = 2.9$
$R_{CC_{min}}(\text{Å}) = 1.7$	$R_{CC_{max}}(\text{Å}) = 2.0$
$N_{min}^{M} = 2.0$	$N_{max}^{M} = 6.0$

Table S7. Parameters for C-M_{1st} interactions using Morse type potentials with a pure Pt catalyst.

Parameters for C-M_{1st} bonds	
$D_{e1}(eV) = 3.41$	$R_{e1}(\text{Å}) = 1.93$
$D_{e2}(eV) = 3.98$	$R_{e2}(\text{Å}) = 0.9$
$C_D = 1.20$	$C_R = 0.22$
$S = 1.17$	$\lambda = 0.08$

All the bonding configurations between carbons and elemental Pt catalyst are displayed in Fig. S3. Especially, (4,4) and (7,0) are representatively used to confirm how the modified potential

describes the bonding structures at the edges of the finite-sized carbon nanotubes with pure Pt catalyst, and the PES fits against DFT energies.

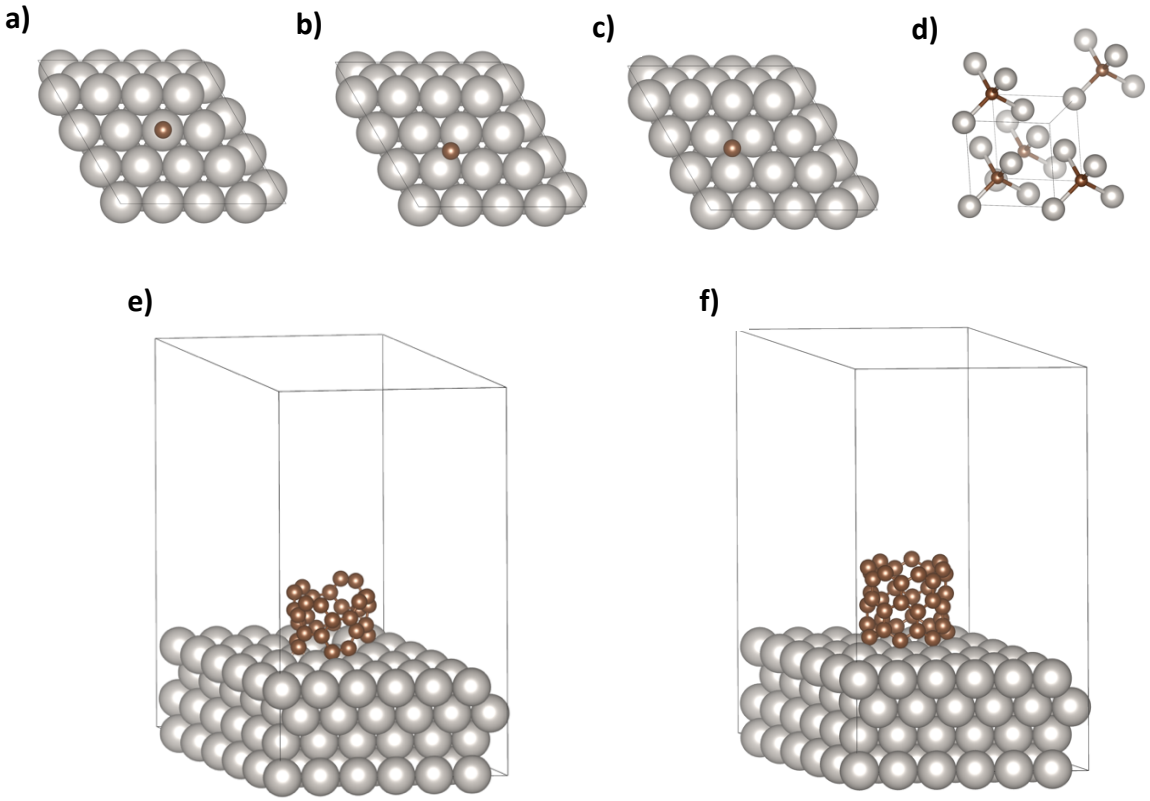

Fig. S3 Bonding configurations for C-M_{1st} interactions between carbons and only Pt(111) catalyst: **a)**, **b)**, and **c)** C_1, **d)** C_1 in pure Pt bulk catalyst, **e)** (4,4), **f)** (7,0). Carbons displayed in **a)**, **b)**, **c)**, **e)**, **f)** are all on the surface of Pt catalyst.

In Table S8 and Fig. S4, bond formation energy patterns obtained from different bonding positions between the selected carbons (i.e. C_1, (4,4), and (7,0)) and Pt single catalyst are shown.

Table S8. C-M_{1st} bond formation energies (E_f) between C_1, (4,4), and (7,0) and only Pt elemental catalyst.

Species	$N_j^{C_{1st}}$	$N_j^{C_{2nd}}$	$N_j^{M_{1st}}$	$E_f(eV)^*$		Error (%)
				new FF	PBE	
C_1	0	0	1	-5.62	-5.09	10.28
C_1	0	0	2	-5.82	-6.51	10.64
C_1	0	0	3	-7.49	-7.21	3.93
C_1	0	0	4	-7.97	-7.60	4.88
(4,4)	2,3	3,5	1,2,3	-25.43	-25.53	0.43
(7,0)	2,3	4,6	1,2,3	-36.42	-36.56	0.38

$* E_{f(C-M)} = E(N * C + N * M_{1st}) - E(N * C) - E(N * M_{1st})$ where N is the number of atoms for each of carbon and a metal component such as Pt in this research.

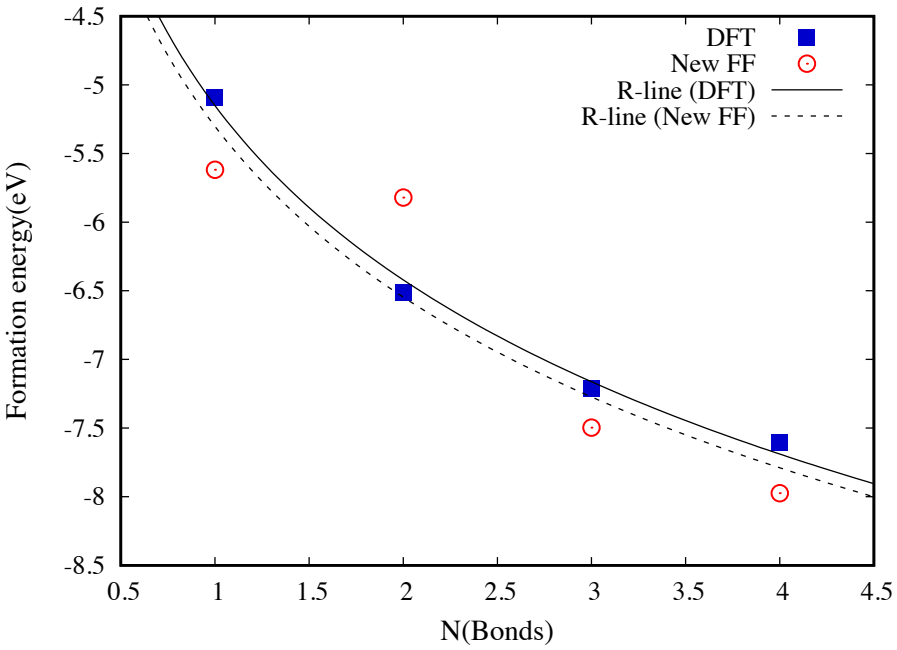

Fig. S4 Bond formation energy pattern of C_1 bonding configurations based on Pt elemental catalyst in the fitting data set, as calculated with the new Force Field, compared to DFT energy pattern showing the nonlinear regression.

- **C-M_{2nd} interactions based on only Cu catalyst**

In using pure Cu catalyst for the C-M_{2nd} interactions described by the new FF, all the necessary parameters provided in Table S9 and Table S10 were adjusted to estimate the energetics derived from the C-M_{2nd} and C-C interactions which take place at the different bonding configurations between C_1, (3,3), and (5,0) and pure Cu metal catalyst.

Table S9. Parameters for $f^{CM_{2nd}}(r_{ik})$, $f^{CC}(r_{ij})$, and α_{ij}^{CC} term reflecting the presence of elemental Cu catalyst here named M_{2nd}.

$R_{CM_{2nd,min}}(\text{Å}) = 2.3$	$R_{CM_{2nd,max}}(\text{Å}) = 2.8$
$R_{CC_{min}}(\text{Å}) = 1.7$	$R_{CC_{max}}(\text{Å}) = 2.0$
$N_{min}^{M} = 2.0$	$N_{max}^{M} = 6.0$

Table S10. Parameters for C-M_{2nd} interactions using Morse type potentials with elemental Cu catalyst.

Parameters for C-M_{2nd} bonds	
$D_{e1}(eV) = 2.8$	$R_{e1}(\text{Å}) = 1.85$
$D_{e2}(eV) = 2.1$	$R_{e2}(\text{Å}) = 0.92$
$C_D = 0.98$	$C_R = 0.1$
$S = 1.12$	$\lambda = 0.08$

All structural configurations between carbons and elemental Cu catalyst are shown in Fig. S5. Especially, (3,3) and (5,0) were representatively chosen to confirm how the new modifications contribute to the descriptions of the bonding structures at the edges of the finite-sized carbon nanotubes with pure Cu catalyst, and the PES fits against DFT energies.

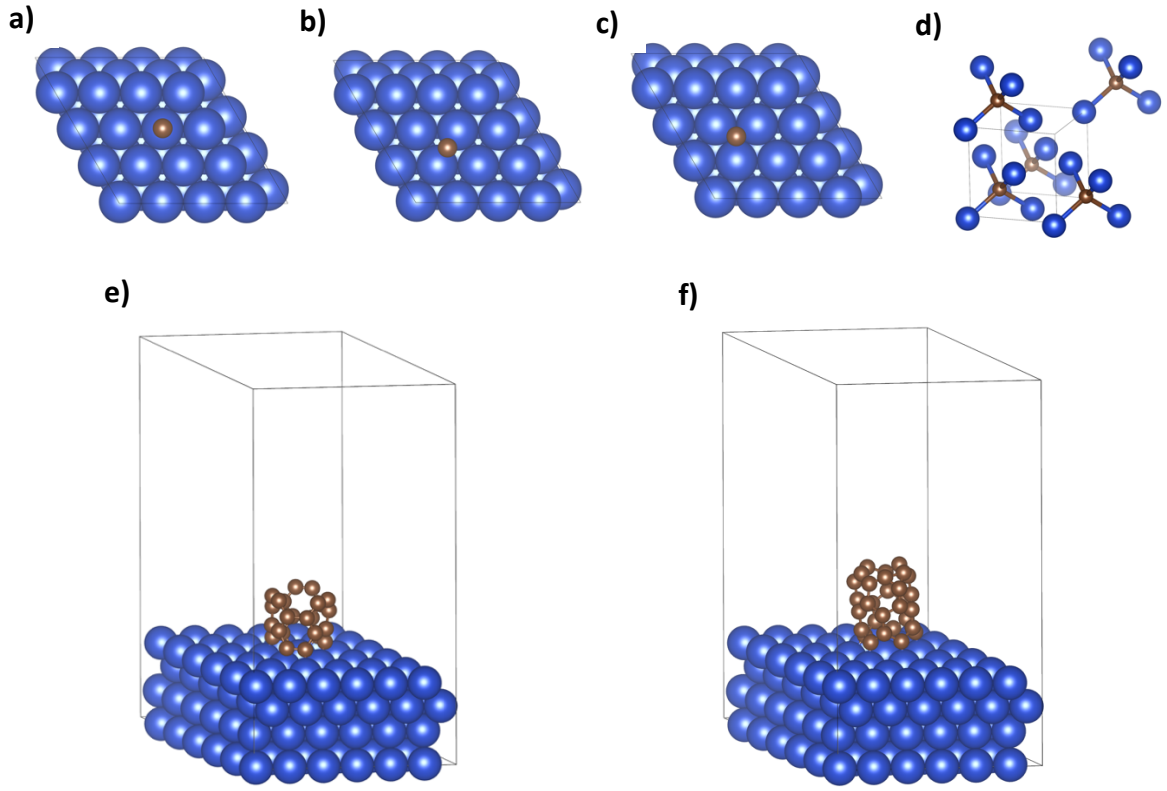

Fig. S5 Bonding configurations for C-M interactions between carbons and only Cu(111) catalyst: **a)**, **b)**, and **c)** C_1, **d)** C_1 in pure Cu bulk catalyst, **e)** (3,3), **f)** (5,0). Carbons displayed in **a)**, **b)**, **c)**, **e)**, **f)** are all on the surface of Cu catalyst.

Bond formation energy patterns made by different bonding positions between the selected carbons (i.e. C_1, (3,3), and (5,0)) and Cu single catalyst are provided in Table S11 and Fig. S6.

Table S11. C-M_{2nd} bond formation energies (E_f) for C_1 and (3,3) and (5,0) only based on Cu elemental catalyst.

Species	$N_j^{C_{1st}}$	$N_j^{C_{2nd}}$	$N_j^{M_{2nd}}$	$E_f(eV)^*$ new FF	$E_f(eV)^*$ PBE	Error (%)
C_1	0	0	1	-4.22	-3.99	5.56
C_1	0	0	2	-5.03	-5.31	5.31
C_1	0	0	3	-6.17	-5.76	7.00
C_1	0	0	4	-6.33	-6.33	0.08
(3,3)	2,3	3,5	1,2,3	-17.28	-17.29	0.00
(5,0)	2,3	4,6	1,2,3	-24.11	-24.33	0.92

$* E_{f(C-M)} = E(N*C + N*M_{2nd}) - E(N*C) - E(N*M_{2nd})$ where N is the number of atoms for each of carbon and a metal component such as Cu in this research.

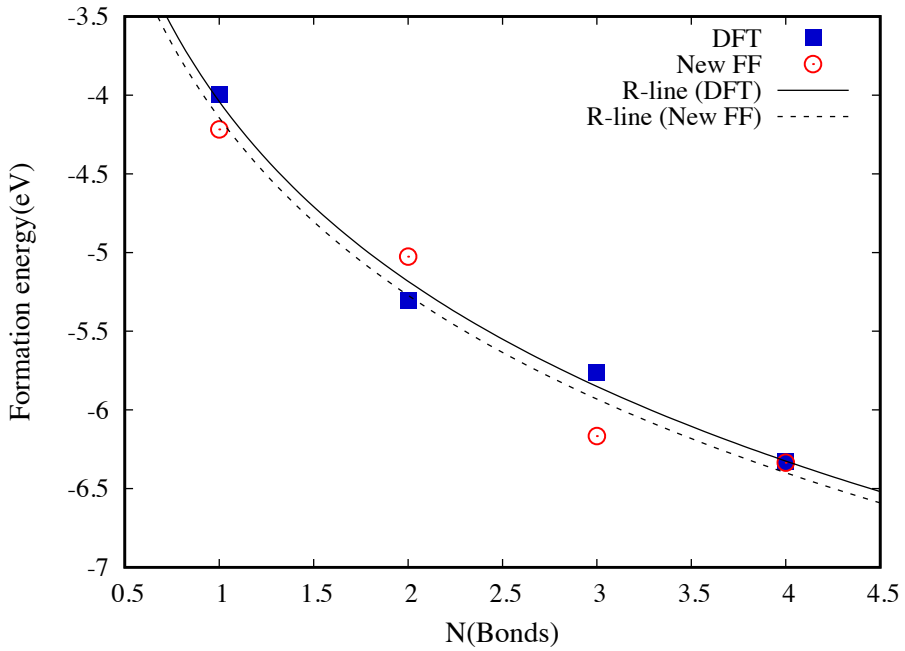

Fig. S6 Bond formation energy pattern of C_1 bonding configurations based on Cu elemental catalyst in the fitting data set, as calculated with the new Force Field, compared to DFT energy pattern showing the nonlinear regression.

■ MD simulations of carbon nanotube growth with Pt-Cu alloy catalyst

- **Carbon nanotube growth using Pt-Cu alloy catalyst**

Characteristics of the chiral and diameter selectivity of the tubes grown have been spontaneously determined by C-C, C-M_{1st} / C-M_{2nd}, and M-M interactions, based on bimetallic alloy catalyst (i.e. Pt-Cu), which are the main feature of the newly modified potential. In this study there are various starting carbon materials to be used for MD simulations; a) carbon

nucleation (i.e. a carbon seed), b) two dimensional C_{24}, c) a group of fullerene such as $C_{80}(D_{5d})$, $C_{90}(C_{2v})$, and $C_{100}(D_2)$ that were cut off more like a hemisphere to be used as a precursor, d) one closed CNT cap that has 86 atoms containing a local defect in an initial geometry, and e) the other closed CNT cap that includes 102 atoms without any topological defect as a precursor. The ratio of binary alloy catalyst from Pt to Cu is 1 to 1 as using a liquid cluster for the atomistic simulations of the CNTs growth.

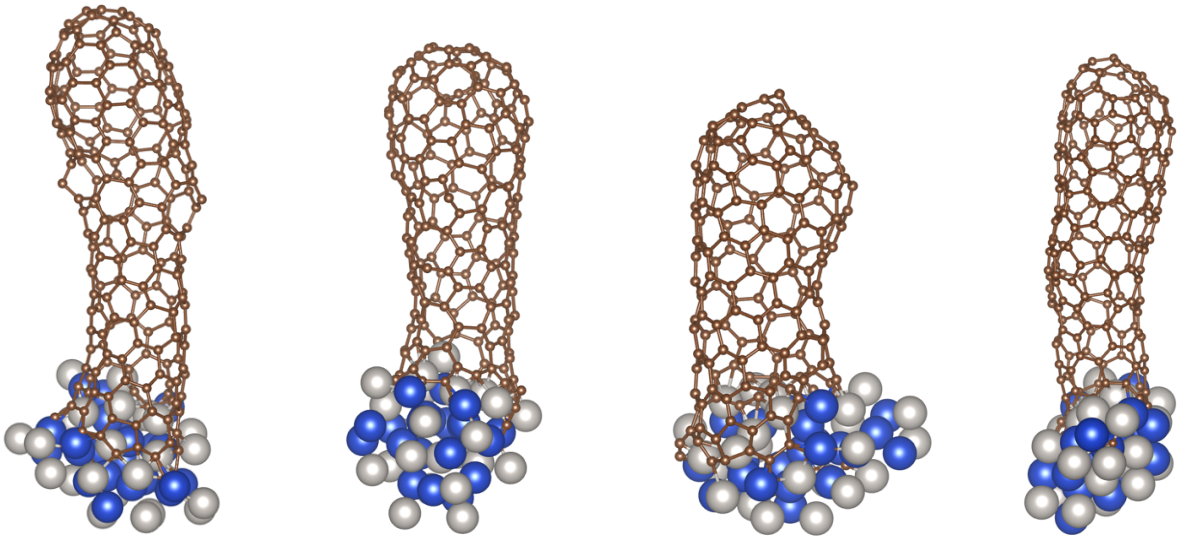

a. (5,3) b. (6,3) c. (6,3) d. (7,3)

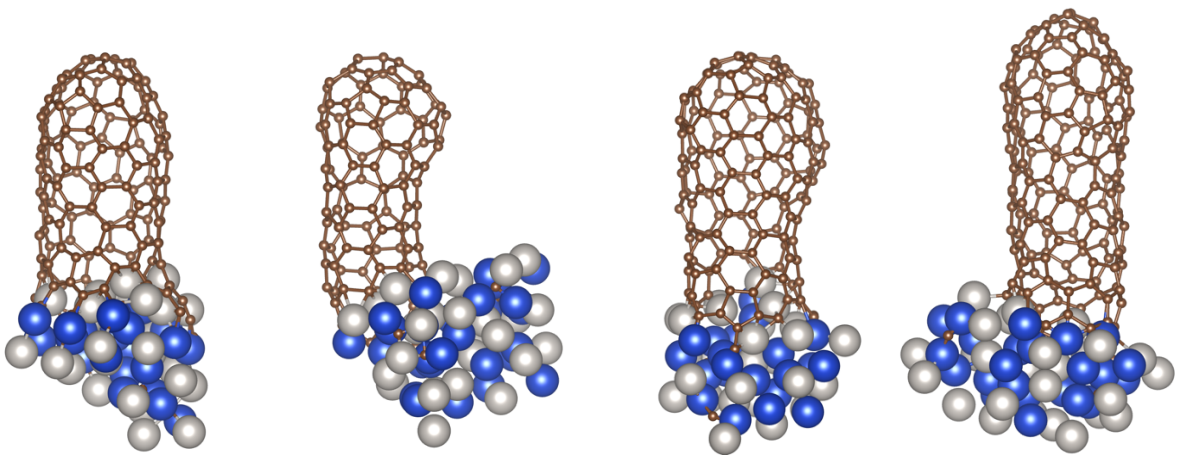

e. (8,3) f. (4,4) g. (5,5) h. (5,5)

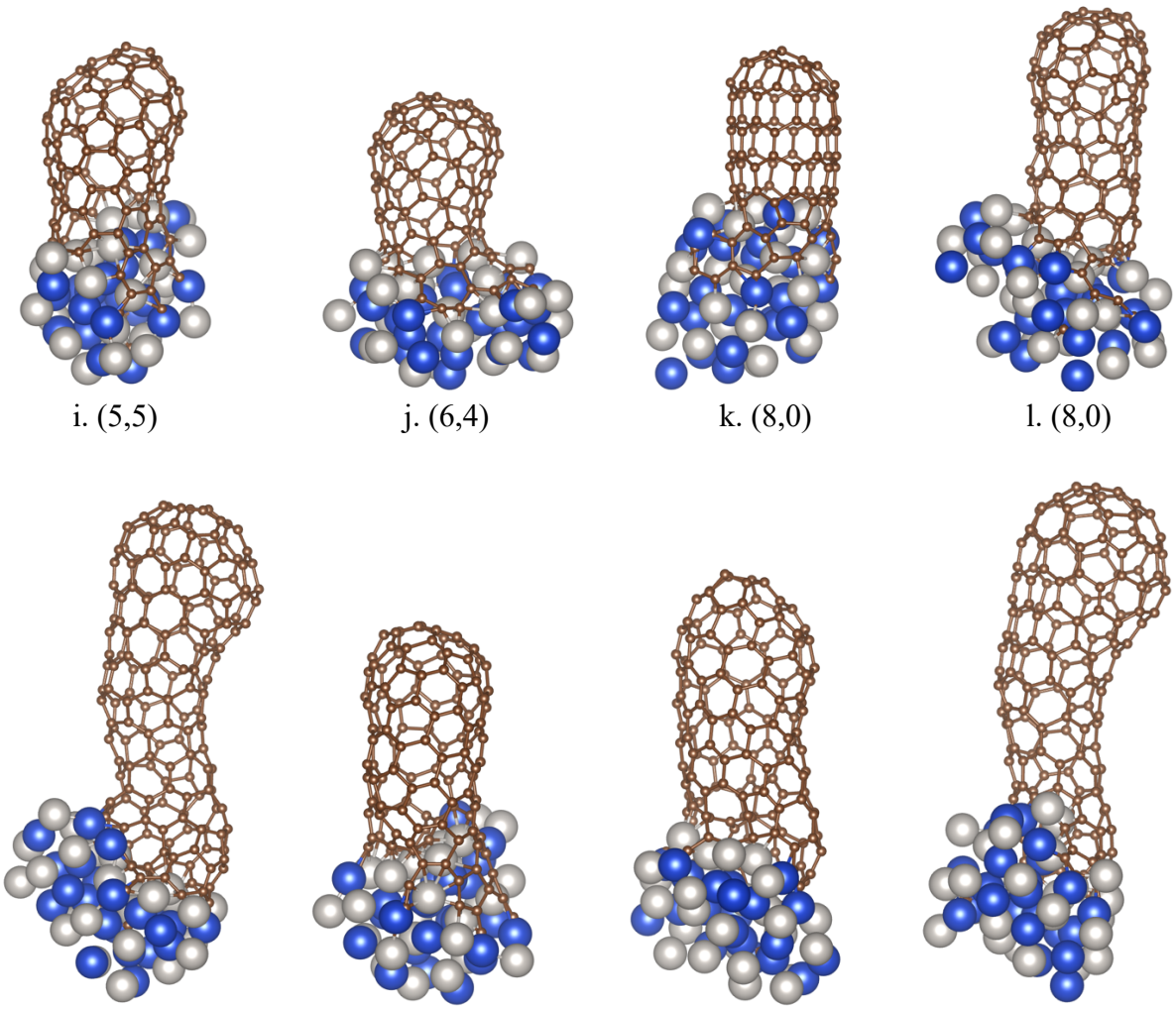

Fig. S7 Snap shots (a.~ e. and g.~ p.) obtained from MD simulations of the CNTs growth using mainly Pt_{27}-Cu_{27} and Pt_{28}-Cu_{28} alloy catalyst.

- **Carbon nanotube growth using only Pt catalyst**

For the validation of MD simulations using pure Pt catalyst in the developed potential, the tubes growth starting from carbon nucleation or a closed CNT cap including 102 atoms without any topological defect in an initial geometry as precursors has been characterized by modelling C-C, C-M_{1st}, and M-M interactions, only based on Pt catalyst. Pt_{54} having the same number of atoms as those of Pt_{27}-Cu_{27} catalyst was used for the CNTs growth simulations.

a. (10,0) b. (12,0)

Fig. S8 Snap shots (a. and b.) obtained from MD simulations of the CNTs growth using Pt_{54} elemental catalyst.

- **Carbon nanotube growth using only Cu catalyst**

Using the new FF code, the validation of MD simulations with pure Cu catalyst has been conducted. Specifically, the tubes growth originated from carbon nucleation or two closed CNT caps including 102 atoms without any topological defect in an initial geometry as precursors has been characterized by modelling C-C, C-M_{2nd}, and M-M interactions, only based on Cu catalyst. Cu_{54} just like Pt_{54} catalyst was used for the atomistic simulations of the tubes growth.

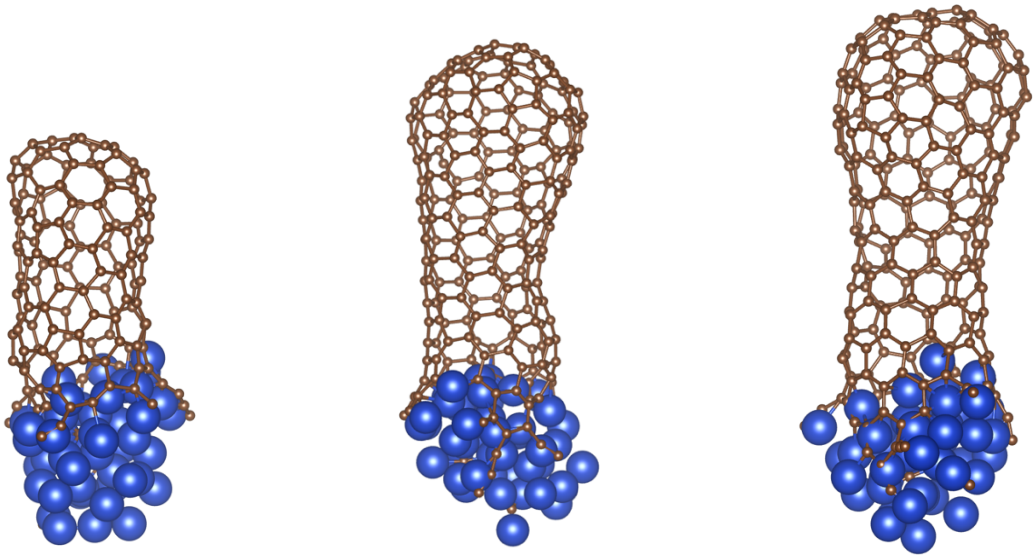

a. (6,6) b. (6,5) c. (10,0)

Fig. S9 Snap shots(a.~c.) obtained from MD simulations of the CNTs growth using Cu_{54} elemental catalyst.

■ DFT calculation details

Density functional theory (DFT) calculations were performed within the Generalized Gradient Approximation Perdew-Burke-Ernzerhof (GGA-PBE)[7], as implemented in the Vienna ab Initio Simulation Package (VASP)[8-10]. The projector-augmented wave (PAW) method with a planewave basis set was used to describe the interaction between the core and valence electrons. Valence electron configurations are $2s^2 2p^2$for C, $4f^{14}5d^9 6s^1$ for Pt, and $3d^{10}4s^1$ for Cu. The electronic eigenfunctions were expanded in the plane wave basis set with an energy cut-off of 400 eV for carbon materials with Pt_3Cu, 295.446 eV for Pt_3Cu and Pt only, and 230.283 eV for Cu only. The energetics of all atomic configurations by geometry optimizations were calculated from the full relaxations of all constituent atoms for bulk, and the three top atomic layer relaxations of Pt_3Cu surface with carbon materials, which are sufficient to find the most stable binding configurations, using the conjugate gradient (CG) method until the residual forces on each atom reached to less than $2 \times 10^{-2} eV/\text{Å}$. The convergence threshold of the total energy was set to $1 \times 10^{-4} eV$ as a default value. The Pt_3Cu (111) surfaces with 4×4, 6×6 , and 8×8 unit cells were used for a periodic slab geometry in which each slab is made up of four atomic layers and the vacuum spacing is more than 15 Å. For Brillouin zone integrations of the Pt_3Cu crystal metal alloy, a $3 \times 3 \times 1$ mesh of *k* points in Monkhorst-Pack scheme was employed. The geometry-optimized atomic configurations by the DFT method were also used for the potential energy evaluations by the new FF model.

■ Reference

1 D. W. Brenner, O. A. Shenderova, J. A. Harrison, S. J. Stuart, B. Ni, and S. B. Sinnott, *J. Phys.: Condens. Matter.*, 2002, **14**, 783.

2 H. Rafii-Tabar and A. P. Sutton, *Philos. Mag. Lett.*, 1991, **63**, 217.

3 A. Martinez-Limia, J. Zhao and P. B. Balbuena, *J. Mol. Model.*, 2007, **13**, 595.

4 Z. Xu, T. Yan, and F. Ding, *Chem.Sci.*, 2015, **6**, 4704.

5 A. P. Sutton and J. Chen, *Philos. Mag. Lett.*, 1990, **61**, 139.

6 G. J. Ackland, M. W. Finnis and V Viteck, *J. Phys. F: Met. Phys.*, 1988, **18,** L153.

7 J. P. Perdew, K. Burke, and M. Ernzerhof, *Phys. Rev. Lett.*, 1996, **77**, 3865.

8 G. Kresse, J. Hafner, *Phys. Rev. B*, 1993, **47**, 558.

9 G. Kresse, J. Furthmuller, *Comput. Mater. Sci.*, 1996, **6**, 15.

10 G. Kresse, J. Furthmuller, *Phys. Rev. B*, 1996, **54**, 11169.